Calorimeter Facilities

1981 Phys. Scr. 23 397

(http://iopscience.iop.org/1402-4896/23/4A/011)

Physica Scripta, Vol. 23, 397–408, 1981

Calorimeter Facilities

A. Astbury

Rutherford Lab, Didcot, Oxfordshire, England

Received November 24, 1980; accepted November 25, 1980

Abstract

The aim of this talk is to provide an introduction to calorimetry on which the following more specialized presentations can build. I shall be selective in the choice of Calorimeter Facilities; strictly speaking there are only two in existence at storage rings, MARK-J at PETRA and MAC at PEP, each having the distinction of including hadron calorimetry. The examples chosen will all be taken from the storage ring environment, where the conditions are quite different from those which prevail at fixed target facilities. The apparatus sits in the centre of mass, consequently the average energy of the particles is lower and they enter the calorimeters at large angles to the normal. Each example will be used to illustrate the basic principle of a method of calorimetry or readout.

The outline of the talk is as follows:

(1) What is a calorimeter?
(2) Facilities MARK-J.
JADE-lead glass.
TASSO-liquid argon.
MAC-proportional chamber readout.
AFS (R807)-uranium and BBQ readout.
UA2-BBQ readout.
(3) UA1 (a) energy calibration,
(b) low energy response,
(c) the problems associated with attempts to cover 4π solid angle.
(4) LEP physics and calorimetry.
(5) Summary and conclusions.

1. What is a calorimeter?

The word calorimeter suggests a device aimed at measuring changes in temperature, however a simple calculation shows this to be extremely impractical. The modularity of part of the UA1 hadron calorimeter, is 1.0 x 1.0 x 0.05 m of iron plus 1 cm of PLEXIPOP, repeated 16 times in depth. An incident hadron of 40 GeV raises the temperature of this whole device by 10^{-15} °C. Fortunately the "heat" can be measured indirectly, from the ionization of the atoms in the medium, either by collecting the charge produced, by measuring the light from energy loss in scintillator, or in some instances, detecting Čerenkov light. Ideally one seeks to absorb and detect all the energy in an active medium; with a few exceptions [NaI, and Lead glass] this proves to be impractical and the cascade is sampled. If the incident particle is an electron or a photon one is concerned with the radiation length of the material and the secondary particles are also electrons and photons. Typically in an electromagnetic calorimeter 13–20% of the energy is sampled in the active medium. With an incident hadron the interaction length becomes the interesting unit and secondary particles include photons as well as hadrons.

If the energy loss by dE/dx in a sample step (absorber + active medium) is ΔE then clearly, for a totally contained shower derived from an incident energy E_0, the number of samplings $n_s = E_0/\Delta E$. The resolution, $\sigma \sim 1/\sqrt{n_s}$ and so we have the basic equation for the resolution of the calorimeter

$$\sigma \sim \sqrt{\Delta E}/\sqrt{E}.$$

The limit of applicability of this rule of thumb for calorimeters is discussed thoroughly in the presentation of U. Amaldi.

2. Facilities

2.1. *MARKJ* [1]

Figure 1 shows schematically a section through the apparatus, which has been used like the other PETRA detectors to seek new flavours, new leptons, test QED and to study the topology of hadronic events. In addition, the main aim of MARKJ is to measure the charge asymmetry from interference of weak and electromagnetic interactions in the process $e^+e^- \to \mu^+\mu^-$, hence the detector has iron toroids for the muons, around a non magnetic central detector.

The central coordinate device is based on 4 layers of drift tubes, each 300 mm long and 10 mm wide placed perpendicular

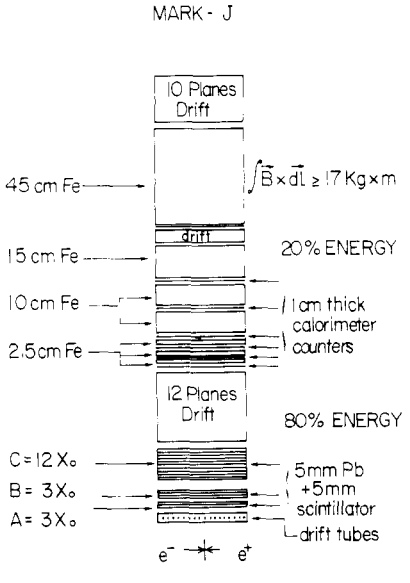

Fig. 1. The layer structure of the MARK J detector as seen by a particle at 90° to the beam axis.

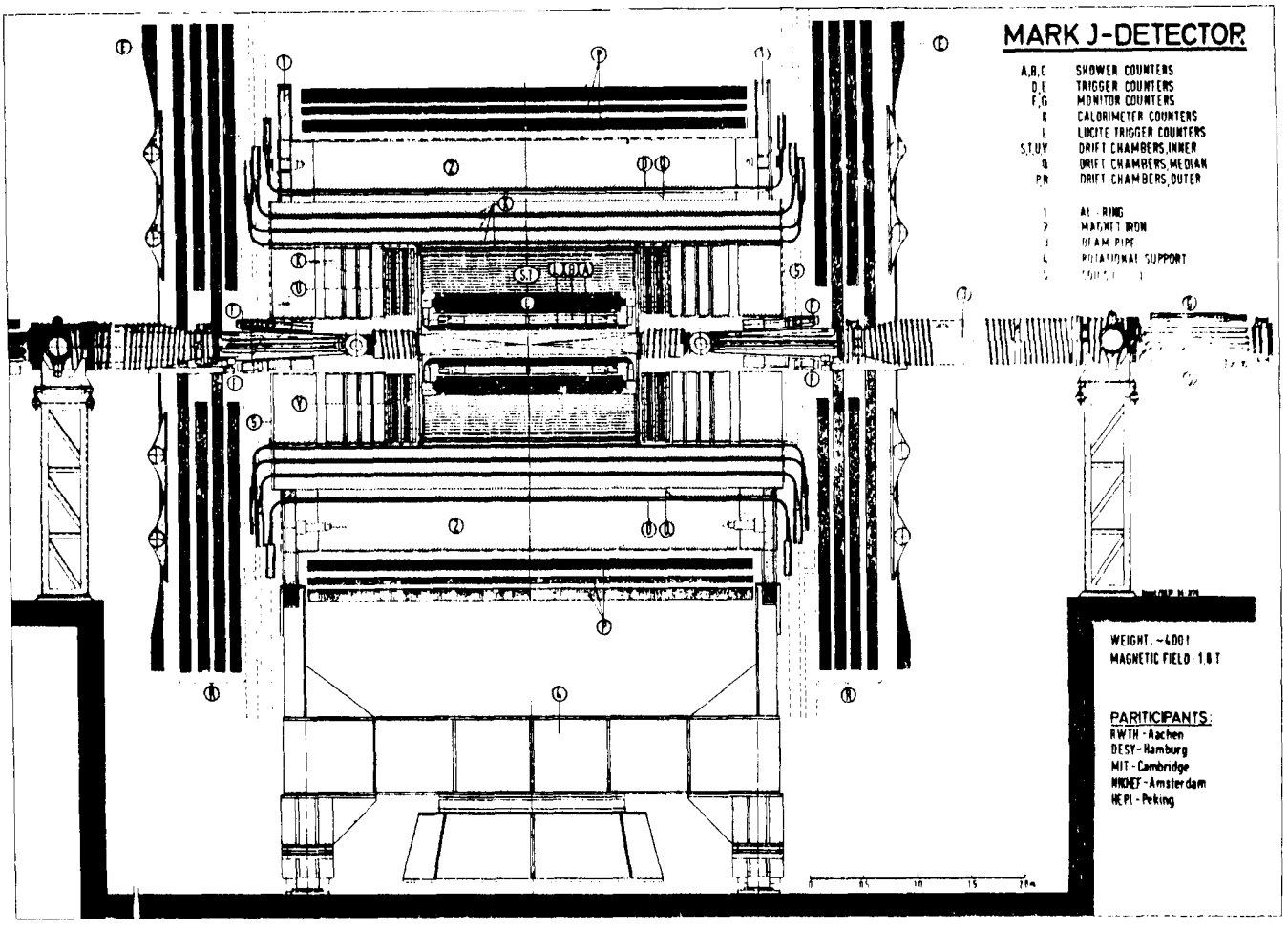

Fig. 2. MARK J – side view.

to the beams and covering the range $30^{\circ} < \theta < 150^{\circ}$. These replace the original lucite trigger counters shown in Figs. 2 and 3. The electromagnetic calorimeter has 18 (3 + 3 + 12) radiation lengths of lead scintillator sandwich (5 mm of scintillator and 5 mm of lead). The counters are 2 m long with conventional light guides and a photomultiplier at each end. The combination of timing and pulse height information yields a precision $\sim 5^{\circ}$ in θ, and the segmentation in ϕ gives a precision of $\sim 7^{\circ}$ for the shower directions. After the drift chamber the hadron calorimeter is based on an iron sampling ranging from 2.5 to 15 cm, and beyond this one has the muon spectrometer. At PETRA energies on average, ~ 80% of the energy is derived from the electromagnetic calorimeter. Figures 2 and 3 show sections through the real detector. In order to obtain the energy calibration, one quadrant (A, B, C, K) was placed in a test beam and the response to e's, π's and μ's measured from 0.5–10 GeV.

The response of the apparatus to large angle Bhabha scatters at $\sqrt{s} = 30$ GeV is shown in Fig. 4 yielding $\sigma \sim 10\%$. The r.m.s. value for hadronic events is ~ 20%. The measurement of visible energy is not used in the fast trigger except for e-pairs when at least 500 MeV is demanded from opposite quadrants of A and B, however it is used extensively in off line filtering. In particular it provides a useful measure of potential background from two photon interactions.

The MARK–J detector is a very conservative device based on standard scintillator and good conventional light collection. It is interesting that it has proved quite competitive in general physics output at PETRA, when compared with the more complex detectors e.g., JADE and TASSO.

2.2. *JADE* [2]

In the JADE detector, Fig. 5, the calorimetric element is an array of lead glass blocks, which measures the electromagnetic energy by detecting Čerenkov light produced by electrons and positrons in the showers. Typically the lead glass used has a radiation length ~ 2.36 cm, a density of 4.08 gm cm^3 and a refractive index of ~ 1.67 for sodium light. The pulse derived from the detector is fast, and a useful feature can be the existence of an energy threshold in the presence of high backgrounds.

The spectrum of the Čerenkov light, $dN \alpha d\lambda/\lambda^2$ implies that one requires a good transmission at short wavelengths which is in conflict with the need for a short radiation length. Poor transmission means that light from different regions of the block produces different response at the photomultiplier and hence worsens the resolution. A typical attenuation length for light is ~ 15 cm at 380 nm.

JADE is built around a solenoid 3.5 m long, 2 m diameter, with an aluminium coil 7 cm thick, producing a field of 0.7 T. Inside the coil a high pressure drift chamber provides track information and some particle identification. Outside the coil there are 30 rings of lead glass blocks (84/ring); each block has an inner surface of 85 x 102 mm, is 300 mm deep, (12.7 radiation lengths) and is viewed by a single 3″ diameter photomultiplier. There are also end caps (192 blocks) and small arrays of lead glass downstream of the experiment which yield luminosity and two photon information. The barrel and end cap arrays cover 90% of 4π.

The blocks were calibrated [90% of them] in an electron beam and yield a resolution of $\pm 6\%/\sqrt{E}$ up to 6 GeV. The

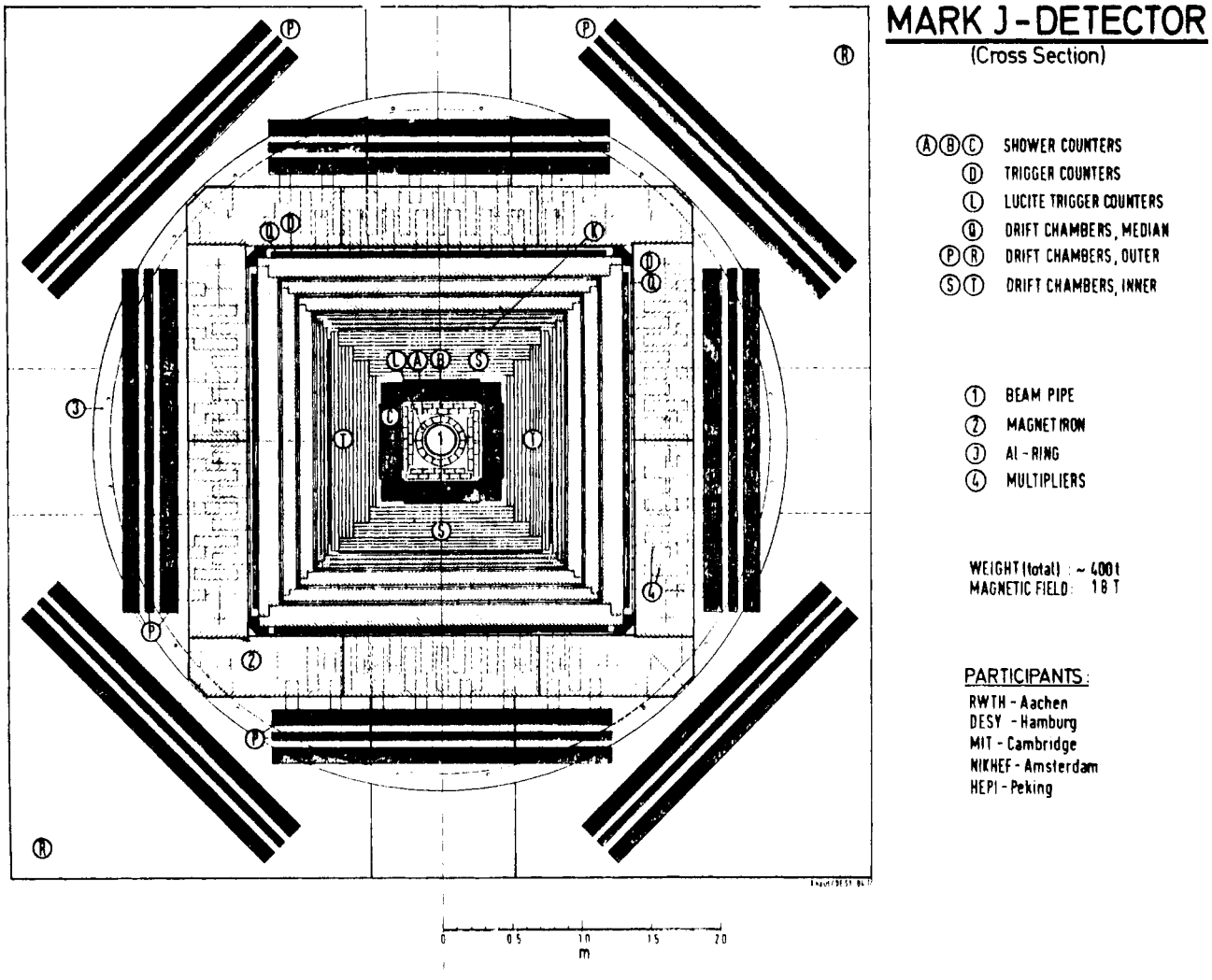

Fig. 3. MARK J – end view.

resolution at 15 GeV is ± 3% where one is almost certainly running into problems of containment – at 5 GeV for example on average ~ 87% of the energy is contained by 12.7 radiation lengths. Figure 6 shows the ratio of the energy measured in a cluster of the lead glass to that of the beam for Bhabha scatters. The device is used in the trigger, and off line the fine grained calorimeter gives an angular resolution of $\Delta\theta \sim 0.6^\circ$ using the known interaction point.

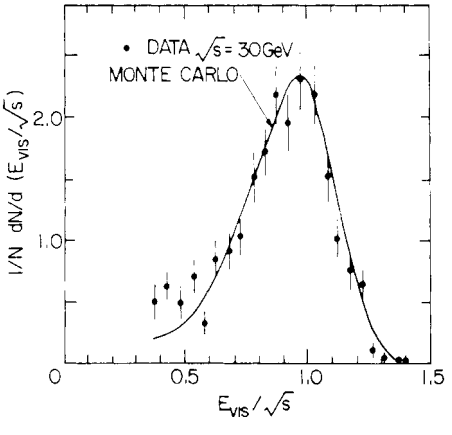

Fig. 4. The energy distribution of hadronic events in MARK J.

2.3. *TASSO* [3]

The electromagnetic calorimeter in TASSO uses liquid argon as the active medium in a sampling calorimeter [4]; the principle of which is shown in Fig. 7. Charge is collected from an ion chamber, without multiplication within the device. In order to achieve a good signal to noise the amount of charge collected must be a reasonable fraction of that released, i.e., the active medium should be a condensed material, which does not attach electrons and has a good electron mobility. Liquid argon meets these requirements but has the disadvantage of needing an operating temperature of − 183°C.

There are considerable electronic problems of noise and of matching the detector capacity to the input of the charge amplifier. The positive ions released contribute very little to the collected charge because of the low mobilities, and signals are small, typically ~ 0.6 pc per GeV. The exclusion of electronegative gases, e.g., oxygen, to a level of ≤ 1 ppm is essential, and the device is reasonably slow, ~ 900 ns for a pretrigger signal. However once the detector is cold, it is very stable, can readily collect charge uniformly from complicated geometries, and is easily calibrated by the injection of a pulse of known charge.

The TASSO detector is shown in Fig. 8; it is built around a solenoid 1.35 m in radius and 4.4 m long, with a thin coil

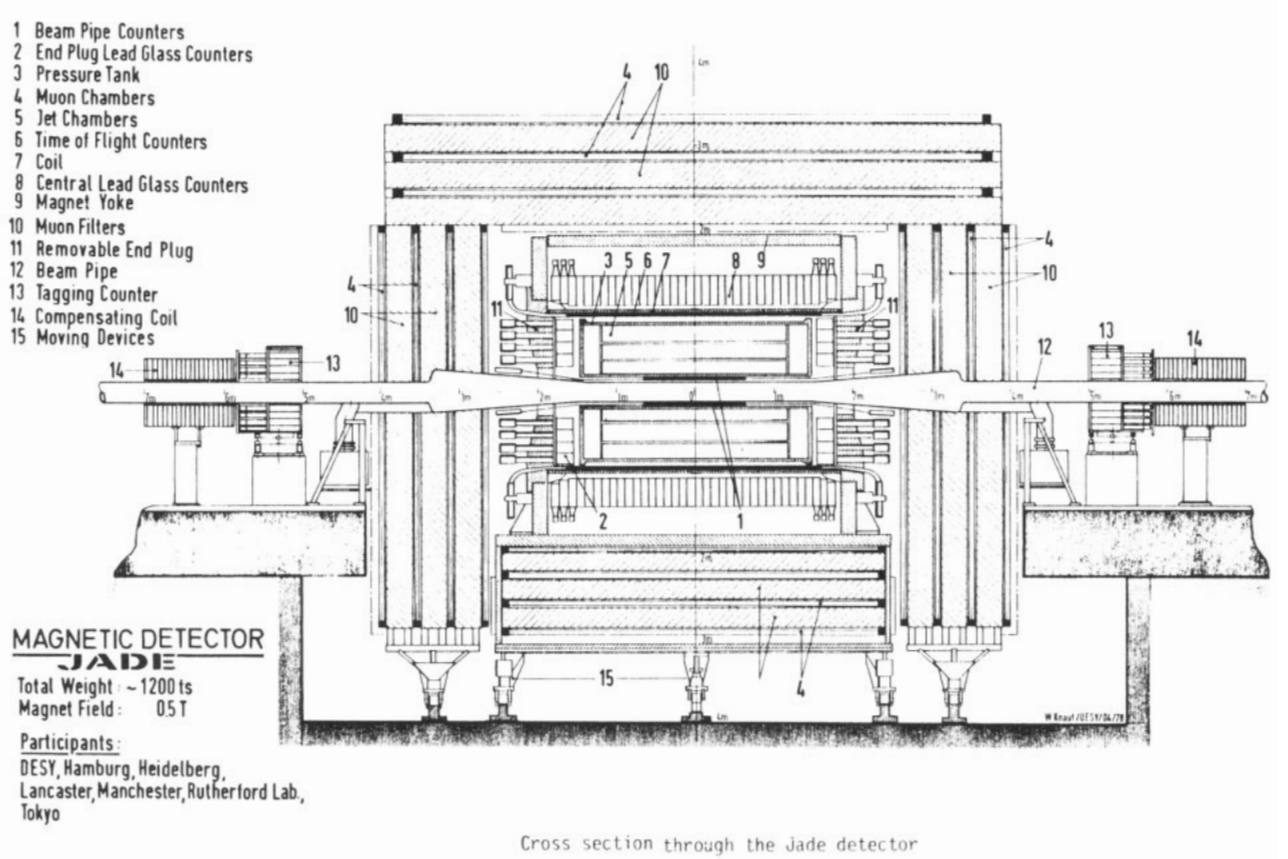

Fig. 5. Cross-section through the JADE detector.

(1 radiation length) producing a field of 0.5 T and containing the central drift and proportional chambers.

We shall be concerned with the liquid argon barrel detectors which cover about 40% of 4π – two thirds of the circumference of the solenoid. These detectors are aimed at measuring the energies of electrons or photon in the range 100 MeV–20 GeV, and providing some pattern recognition such that showers may be unravelled in jets, and their energies measured.

In order to achieve the above aims the geometry, optimised for TASSO, is shown in Fig. 9. It is built from "towers" of lead plates subtending equal solid angles at the interaction point. The basic sampling is 5 mm of liquid argon and 2 mm of lead. The front towers are $7 \times 7\,\text{cm}^2$, placed at 180 cm from the crossing point, and have a solid angle of 1.5 msr. These towers extend for six radiation lengths and each is read into an ADC channel. The back towers are 14 x 14 cm in area and contain eight radiation lengths; each back tower drives an ADC channel. There also exist orthogonal strip electrodes (2 cm wide) which aid pattern recognition. The front part of the detector contains two independent layers of aluminium electrodes and etched copper plate electrodes. These measure the energy of showers which start in front of the detector and dE/dx for charged particles. One stack of the barrel detector is 3.98 m x 0.99 m x 0.45 m and there are 8 of them, requiring 10,928 readout ADC channels. It is interesting to note that during the cool down period of ~ 2.5 days, the 4 m dimension shrinks by some 2 cm. The energy resolution is shown in Fig. 10. The resolution obtained with a realistic amount of material in front of the liquid argon detector (~ 1.3 radiation lengths), as exists in TASSO, is

$$5\%\ (E > 4\,\text{GeV}), \quad 10\%/\sqrt{E}\ (1 < E < 4\,\text{GeV/c}), \quad \text{and}$$

$$\frac{15\%}{\sqrt{E}}\ (E \sim 0.3\,\text{GeV})$$

The spacial localisation in x and y is ~ 4 mm and the device can be run with an r.m.s. noise level of ~ 15 MeV – equivalent

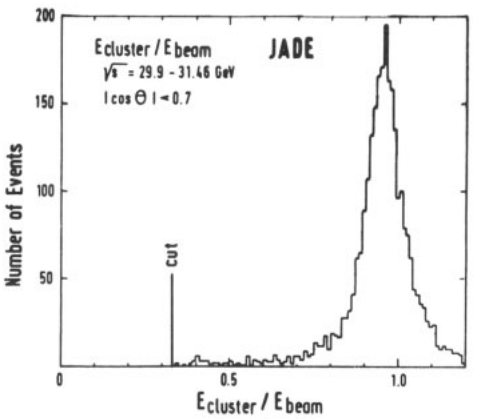

Fig. 6. Distribution of lead glass cluster energy divided by beam energy for Bhabha events. 29.9 GeV $\leqslant \sqrt{s} \leqslant$ 31.46 GeV.

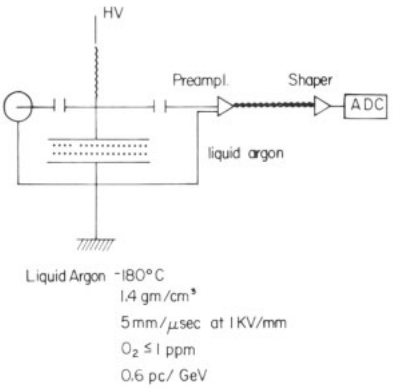

Fig. 7. The principle of the liquid argon detector.

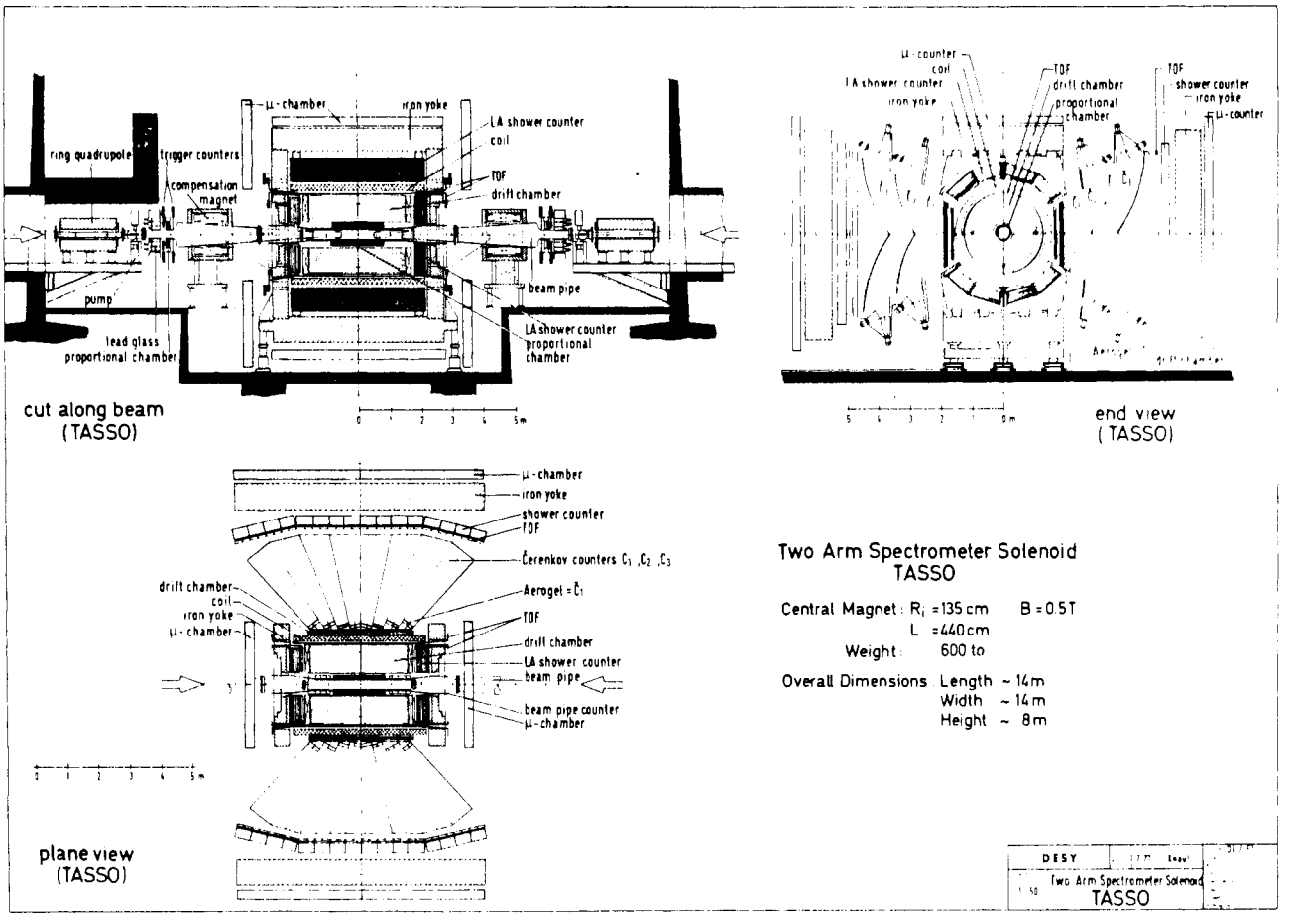

Fig. 8. Different cross-sections of the TASSO detector.

photon energy. This last figure is very similar to the noise level achieved in the upgraded MARK II detector at PEP.

Figure 11 shows a comparison in TASSO, of Bhabha scattering; in one case the momenta are measured in the drift chamber and in the second are derived from the calorimeter. The improvement in performance is very striking.

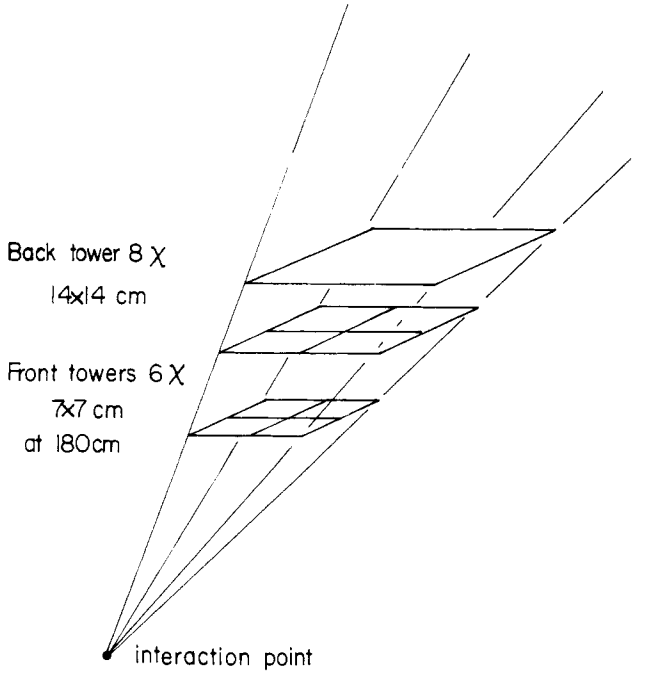

Fig. 9. A schematic view of the "tower" geometry of the liquid argon (barrel) detector in TASSO.

2.4. *MAC detector*

The active element in the calorimetry of the MAC detector is a set of proportional tubes [5]. The layout of the calorimetry is shown schematically in Fig. 12. A 50 μ wire is stretched along extruded aluminium channel, surrounded by an argon (80%) methane (20%) gas mixture and run as a proportional chamber with a typical gas gain of $\sim 10^4$. The longitudinal coordinate is obtained using current division.

In MAC the electromagnetic calorimeter has 2.8 mm thick lead type metal plates, where the plate closes the proportional tube. The hadron calorimeter has iron plates of 2.7 cm thickness and the proportional tube is made entirely in aluminium. The MAC detector, shown schematically in Fig. 13, consists of a central region and two end caps. The central region is built around a solenoid of 0.5 m radius, with an aluminium coil (0.5 radiation lengths) which produces an 0.5 T magnetic field.

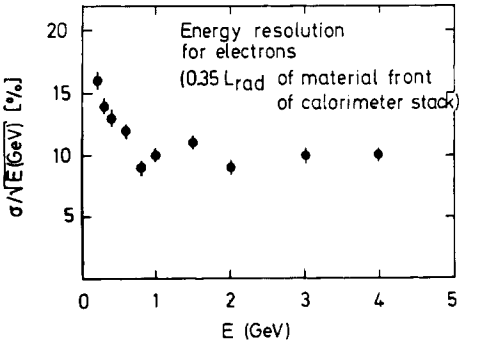

Fig. 10. The energy resolution of TASSO liquid argon detector.

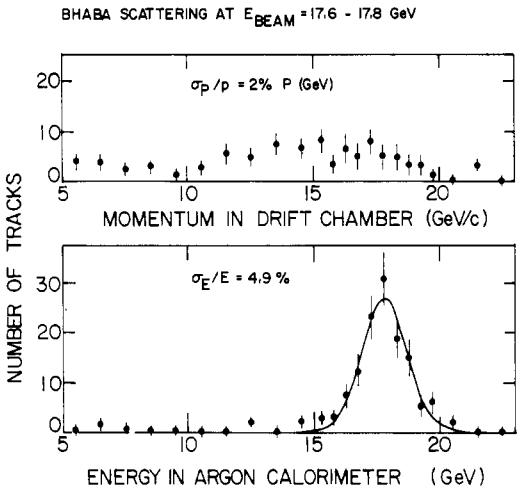

Fig. 11. A comparison in TASSO, using Bhabha scattering, of the momentum resolution obtained from the drift chamber with that of the liquid argon detector.

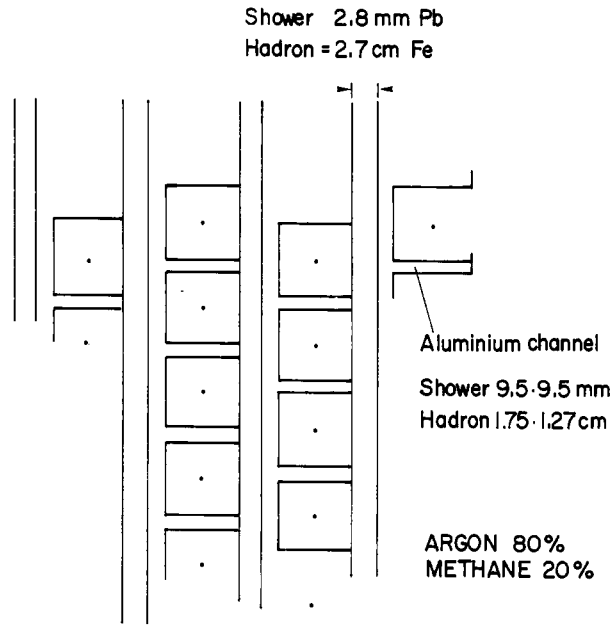

Fig. 12. Cross-section showing schematically the internal detail of the proportional tubes used in the MAC detector.

The drift chamber with a precision of 0.2 mm can determine only the sign of particles at 15 GeV. The electromagnetic calorimeter [36 layers of 2.8 mm lead plates] covers 85% of 4π and is surrounded by the 5.5 interaction lengths of hadron calorimeter (35 layers of 2.7 cm iron plates). The end caps which do not contain electromagnetic calorimetry as such, are readout with horizontal proportional tubes and radial segmentation of cathode planes provide the angular resolution. Copper coils inside the iron produce a toroidal field which with the aid of drift chambers inside the detector and proportional tubes cladding the whole outer surface, can be used as a muon spectrometer.

The arrangement of the readout of the central region of MAC

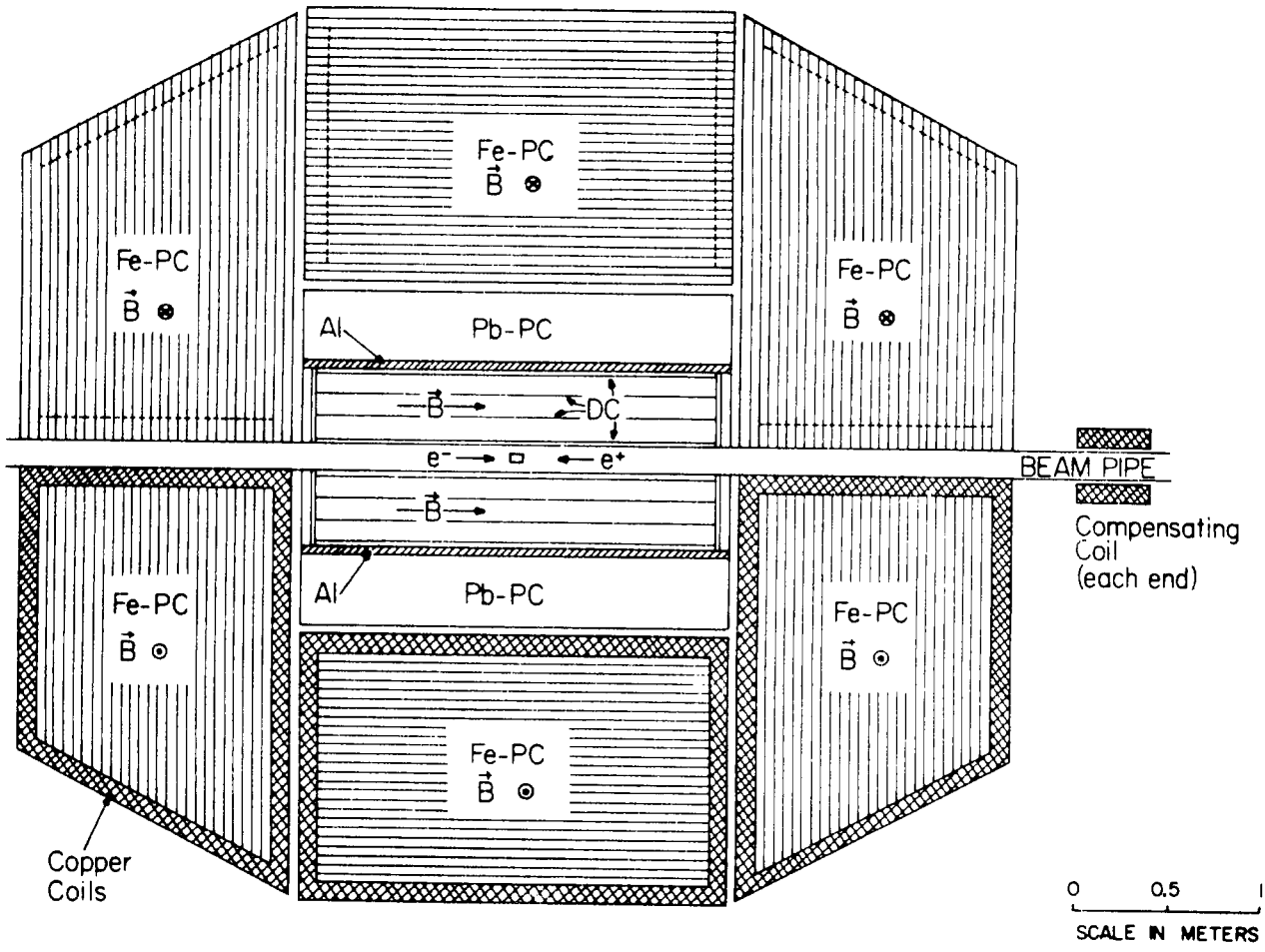

Fig. 13. A cross-section through the MAC detector.

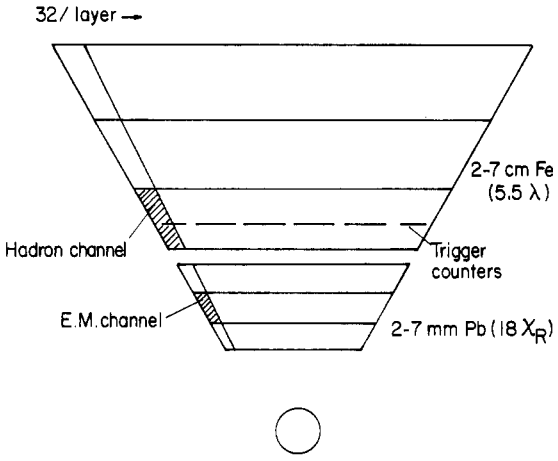

Fig. 14. A schematic view of the organisation of the readout from the central calorimeters in MAC.

is shown schematically in Fig. 14. The proportional tubes run parallel to the beams and are ganged together so that each calorimeter is read in three layers (e.g., 3, 10, 5 radiation lengths). Each layer has 32 bins in ϕ which yields an angular resolution ~ 30 m radians. Current division on all of these tubes in parallel then provides the longitudinal coordinate. The grouping of readout is done to reduce the number of ADC channels required; clearly with many more channels made available the detector has excellent flexibility for pattern recognition in energy flow, should the physics demand it.

Figure 15 shows an artists impression of MAC in the expanded state, i.e., end caps withdrawn. The performance [6] of the calorimeters under test conditions yields $17\%/\sqrt{E}$ for the resolution of the electromagnetic calorimeter in the energy range 0.5–15 GeV, while the hadron resolution is ~ $75\%/\sqrt{E}$ for pions in the range 1–15 GeV. Provision is made to use the information on total observed energy directly in the trigger. The electronic problems are considerable, since the dynamic range of the detector must extend down to a single minimum ionizing particle, and current division has to operate on many wires in parallel. The future performance of MAC at PEP will be watched with great interest since it is the first full ($\sim 4\pi$) calorimeter facility to operate at e^+e^- rings.

2.5. *AFS at ISR (R807)*

Before describing very briefly the AFS it is necessary to introduce the principle of readout using wave length shifter (BBQ)

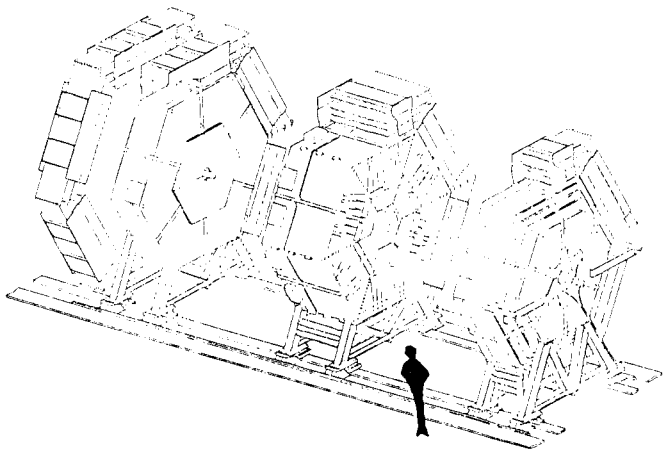

Fig. 15. An artist's impression of the MAC detector.

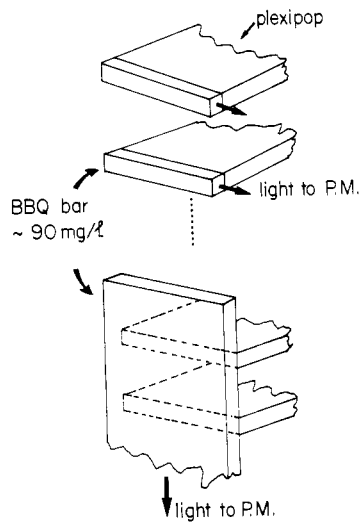

Fig. 16. A schematic view of the principle of readout using BBQ wavelength shifter.

[7]. The active sampling element in many calorimeters is cheap scintillator and the readout problem consists of matching the area of the edges of the scintillator to that of the photocathodes of the photomultipliers, in situations where conventional light guides are not mechanically feasible, and would in any case lead to a prohibitively large number of tubes. Figure 16 shows very schematically the principle of readout via BBQ. Light from the scintillator reaches the edge via internal reflections, it then crosses a boundary (no optical contact) into a BBQ rod or bar which is usually plexiglass doped with BBQ (40–120 mg l^{-1}). Here it is absorbed and re-emitted isotropically at a longer wave

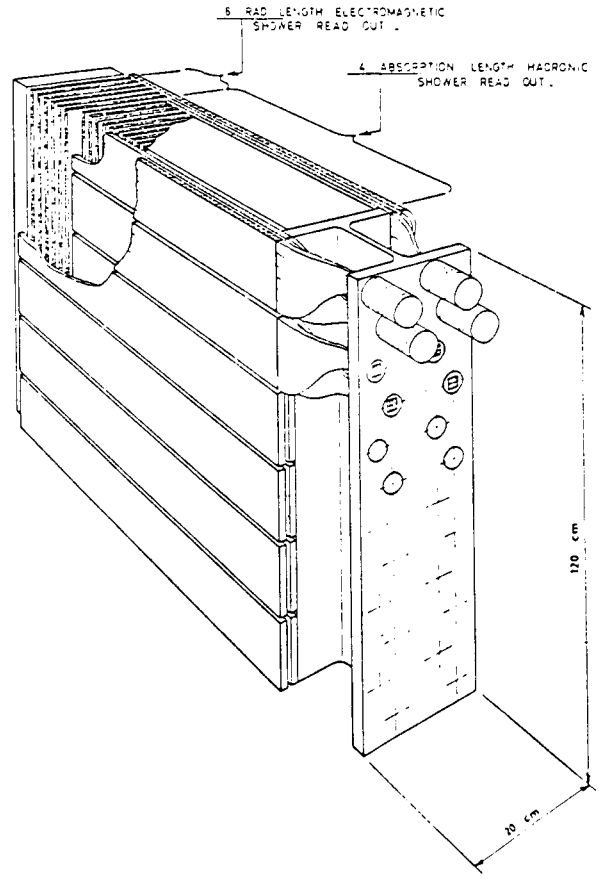

Fig. 17. A sketch of a stack of a module of the uranium calorimeter of the AFS.

length. The re-emitted light can be "piped" to photomultipliers in the conventional way. The matching of wavelengths within the system can present a practical problem since BBQ has an absorption peak at ~ 380 nm which is rather short for some widely used scintillator (e.g., PLEXIPOP has a peak emission at 410 nm) and re-emits at ~ 500 nm which is beyond the peak response in the most widely used bialkali photocathodes. This problem is far outweighed by the versatility offered in complicated geometries. The light from the BBQ is emitted with a lifetime governed by a decay constant $\tau \sim 15$ ns, which necessitates rather wide timing gates in order to collect all the light from calorimeters using this type of readout.

Figure 17 shows a module of the AFS at ISR. Light from the scintillator is converted in BBQ bars and then transmitted to the photomultipliers down perspex light guides. The front section of the module is finely sampled (2 mm of uranium, 6 radiation lengths) and serves as an electromagnetic calorimeter. The rear section, ~ 4 interaction lengths of sheets of 3 mm uranium and 5 mm copper serve as the hadron calorimeter.

In this detector for the first time one meets extensive use of uranium in a calorimeter [$\rho \sim 19\,\mathrm{gm\,cm^{-3}}$, radiation length 0.32 cm, absorption length 12.0 cm]. It has been shown [8] that in uranium one can compensate, on an event by event basis for energy lost in nuclear excitation. In iron the energy lost in nuclear excitation is usually not seen in the detector since it results in short range nuclear fragments, or low energy neutrons which are detected with low efficiency. Fluctuations in the amounts of unseen energy give a worsening of the resolution. Since U^{238} is fissionable by neutrons greater than 1 MeV yielding ~ 2.65 neutrons per fission, one has the possibility of a "built in amplifier" of the number of neutrons, which leads to a compensation for energy lost in nuclear excitation. No more will be said here, since this topic is taken up by later specialist presentations. The improvement in resolution can be a factor ~ 2 better than that obtained with an iron calorimeter employing the same sampling thickness.

The AFS is shown in Fig. 18 in its "2π mode". Each "wall" of the calorimeter consists of 2 x 16 stacks of uranium with finely segmented copper calorimeters filling in the corners. The calorimetry plays an essential roll in the trigger for the experiment which aims to study high P_T physics at ISR – in particular events involving "jet triggers".

The natural radioactivity in the uranium provides a good monitor of performance and response, although probably excludes the use of proportional tubes as the active detector. However test devices using liquid argon have been run successfully.

2.6. *The UA2 detector – planned for $\bar{p}$–p collisions at CERN SPS*

The UA2 calorimetry will be described very briefly indeed. It is included in this review as an excellent example of the compact geometry which can be achieved using BBQ readout. Figure 19 shows the basic module, with an electromagnetic section [17 radiation lengths of lead with 3.5 mm sampling] followed by the hadronic section [3.5 interaction lengths of iron with 1.5 cm sampling]. Both sections are readout via BBQ bars collecting light from either the electromagnetic or hadronic samples. A module under test gave resolutions of $\sim 14\%/\sqrt{E}$ for the electromagnetic and $60\%/\sqrt{E}$ for the hadronic calorimeters; both results were obtained with 1.5 radiation lengths of tungsten in front of the detector to simulate real experimental conditions,

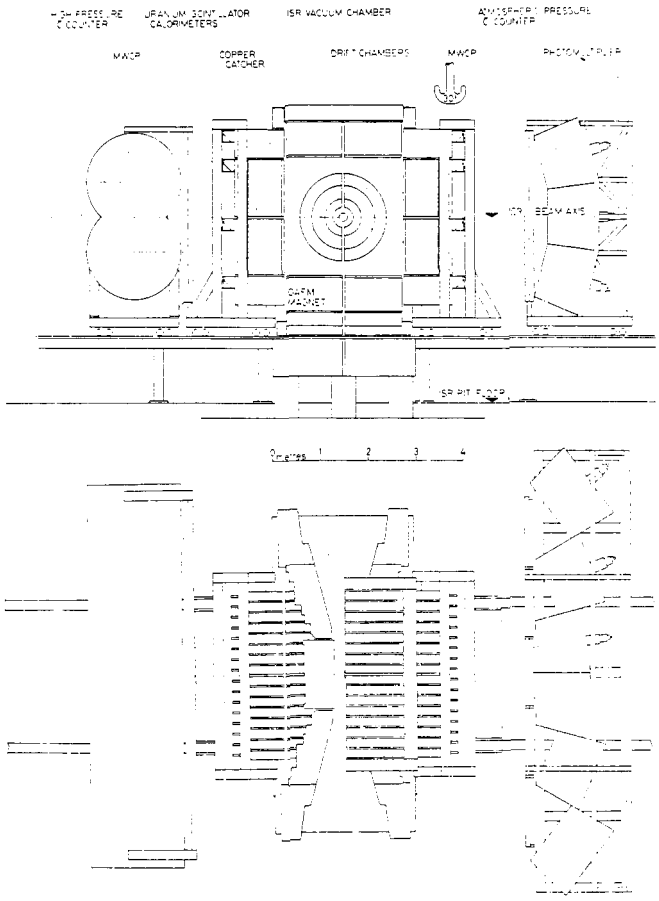

Fig. 18. Layout of AFS-2π calorimeter.

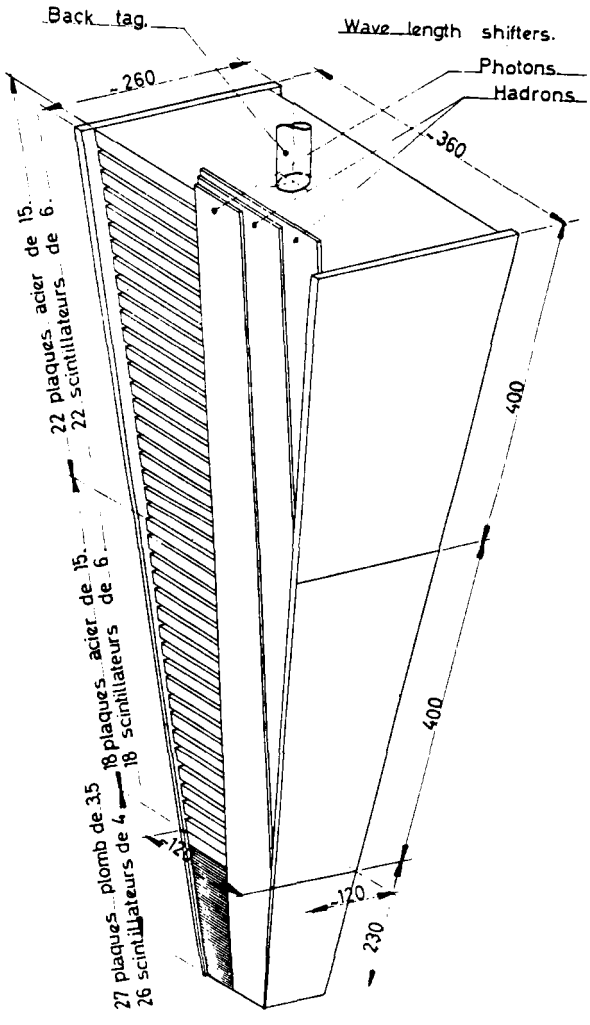

Fig. 19. The basic module of the UA2 calorimeter.

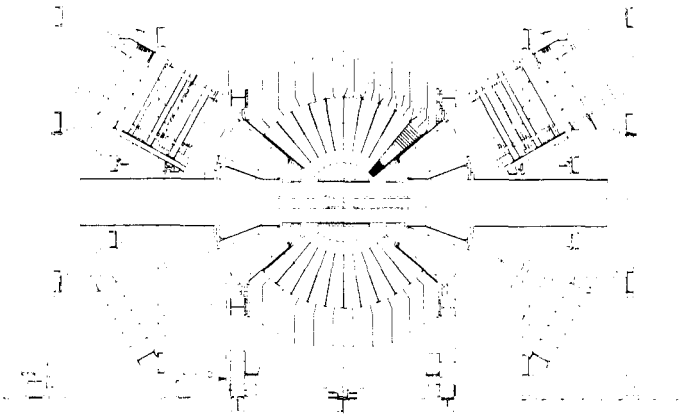

Fig. 20. A cross-section through the UA2 detector.

where a radiator is used to materialize photons in an effort to combat the overlap problem of low energy pions and high energy photons simulating electrons in a detector which has no magnetic field in the central region.

The full UA2 detector is shown in Fig. 20. The simple central detector comprising alternating layers of drift and proportional chambers is surrounded by 240 modules yielding a very uniform geometry between $\theta = 40^\circ$ and 140°, with full coverage in ϕ. Beyond this region a spectrometer with a toroidal magnetic field provides enough bending power to determine the sign of electrons from decays $W^\pm \to e^\pm + \nu$.

3. The UA1 Detector

This is a large detector designed and under construction for the study of $\bar{p}$–p collisions in the CERN SPS. It has the objective, like UA2, of being capable of discovering the quanta of the electro-weak fields, W, and Z° should they exist with masses ~ 90 GeV. However UA1 also aims to have a good general overview of collisions in the new energy range [160 TeV equivalent energy for fixed target physics]. To this end it has a very ambitious coordinate device at the centre, a 6 m x 2.4 m diameter drift chamber with image readout designed to provide a bubble chamber like picture of each event.

Here the detector will be described from the calorimetry point of view with brief reference to some results obtained in testing part of the hadron calorimeter. These results are described in greater detail elsewhere in this conference and their relevance to calorimetry at LEP is emphasized [11].

The UA1 calorimeters are shown schematically in Fig. 21. The degree scale is plotted in a way which shows rapidity since in a hadron collider this represents the scale of particle density. For example if the detectors did not extend to angles $< 5^\circ$ almost half the particles on average would escape detection. The calorimeters in the very forward regions appear "thin", only because all the available space in the straight section between SPS elements has been filled. The particles leaving the interaction region strike first an electromagnetic calorimeter, which in all cases is read out in several depth segments in order to help π/e identification. The relatively thick hadron calorimeter (12.2 interaction lengths) is made from the magnets in the SPS ring which compensate the field of the main 0.7 T diode in the experiment. All of the calorimeters rely on scintillators with BBQ readout.

Figure 22 shows a "beam's eye" view through the UA1 detector, drawn with sections at different depths in order to reveal the different components. Outside the central detector the first calorimeter at large angles follows the geometrical shape of the cylinder. The sampling material and thicknesses are given in Fig. 21. The readout is via BBQ doped perspex bars (4 m arcs). Each counter is 20 cm wide in the beam direction and there are 48 of them. The test results indicate a resolution $\sim 13\%/\sqrt{E}$. The electromagnetic calorimeters at the ends of the detector are shaped like the petals of a flower – 32 at each end covering the region from 25°–5°. The attentuation length of the scintillator is chosen to match – within ~ 10% – the variation of $\sin\theta$, and so transverse energy is read directly. The measured resolution is $\sim 10\%/\sqrt{E_T}$. The central hadron calorimeter is made by inserting scintillators in the laminated (5 cm iron) return yoke of the magnetic. This calorimeter has a measured energy resolution $\sim 80\%/\sqrt{E}$ for contained showers. The dipole field is horizontal, 0.7 T, over a useful volume of 3 m x 3 m x

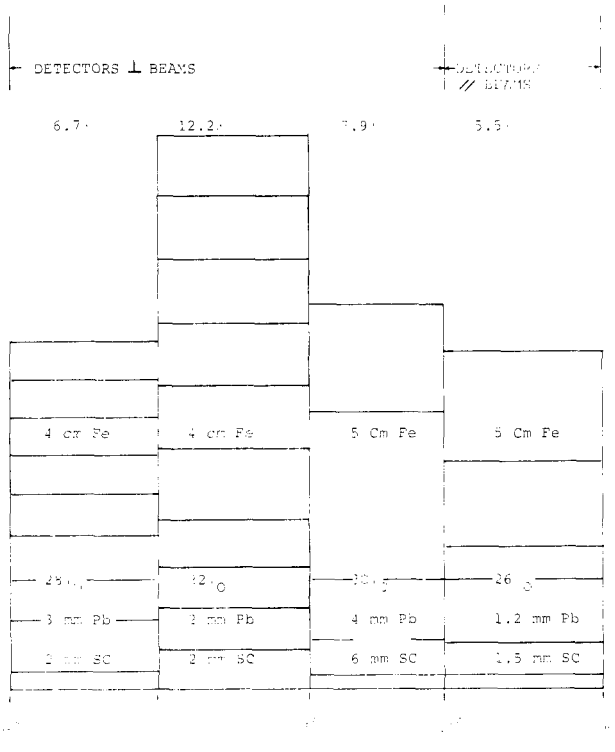

Fig. 21. A schematic view of the electromagnetic and hadron calorimetry in the UA1 detector.

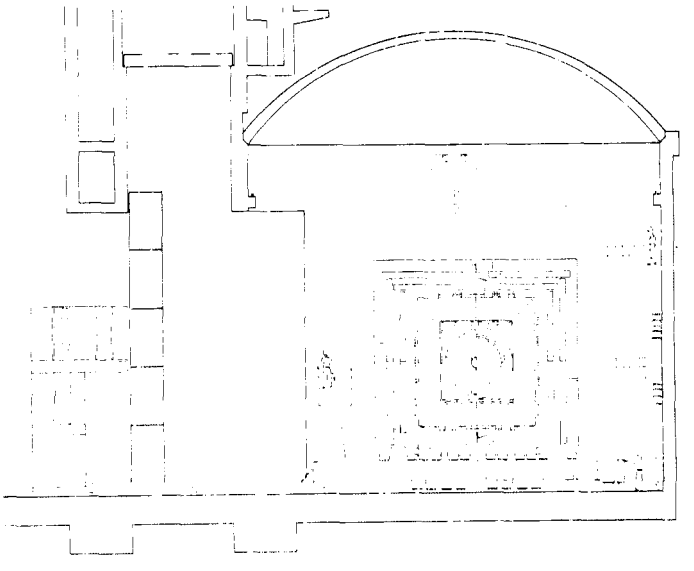

Fig. 22. A beam's eye view of the UA1 detector.

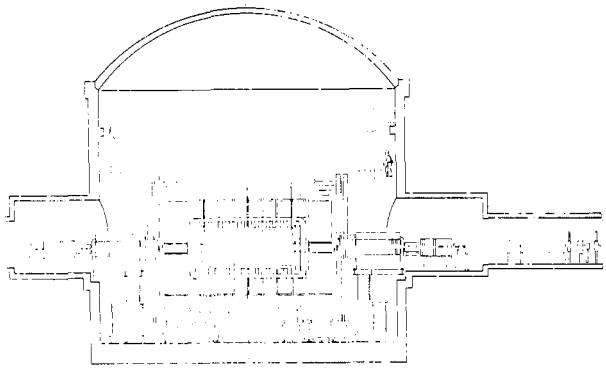

Fig. 23. A longitudinal section through the UA1 detector.

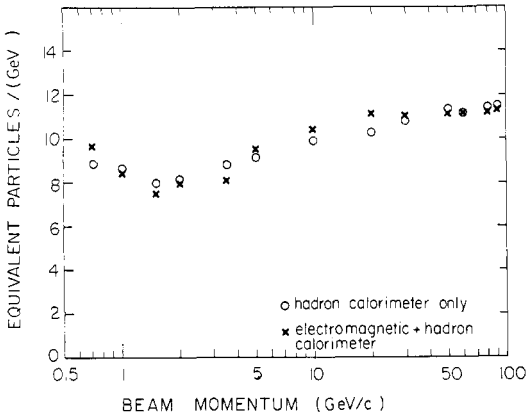

Fig. 24. The number of equivalent particles per GeV for the bare hadron calorimeter of UA1 and the combined calorimeter–electromagnetic plus hadron.

7 m. Also shown in the figure are the two layers of drift tubes which clad the whole detector and use the many interaction lengths of material to provide a muon detector. This extremely interesting capability of μ detection comes in a certain sense, "for free", (although not financially!) when one has built in extensive hadron calorimetry.

A longitudinal section in Fig. 23 reveals the remaining calorimeters, hadronic end caps (5 cm Fe), the calorimetrized compensating magnets with electromagnetic calorimeters in front and then filling in the available space between the magnetic elements of the SPS machine, the very forward detectors. Even further downstream there exist luminosity detectors based on the Roman pot design used so successfully at ISR. In UA1 one has attempted full 4π calorimetry but, as mentioned earlier, it is extremely difficult to collect all the energy from each interaction. The e^+e^- collisons with a characteristic distribution of $1+\cos^2\theta$ for single photon events present a less difficult problem.

I would like to refer very briefly to three questions concerning the UA1 calorimetry which have arisen during the testing of prototypes of the hadron calorimeter, this work is described in more detail in Corden et al. [11].

3.1. *Energy calibration*

Almost all calibrations involve the use of muons to derive a quantity usually referred to as an "equivalent particle". If the charge derived from a muon traversing the whole detector is measured, then knowing the relative proportion of active and inactive material one can obtain the energy calibration. However care must be taken to ensure that the most probable energy deposition for the muon is not a function of muon momentum. In the UA1 case, where several samplings are added together, the peak shifts by ~ 0.22%/GeV. This is due to the fact that the relatively rare processes like δ-rays, pair production and bremsstrahlung which normally lead to an increase in mean energy deposited, when added, can increase the most probable value. The UA1 hadron calorimeter uses $\lesssim 5$ GeV/c muons to fix the energy scale.

3.2. *Low energy response*

Ideally the response of the calorimeter over its whole working range should be linear, so that for example 40 GeV jet produces the same response as a single 40 GeV pion. Figure 24 shows the response for the UA1 hadron calorimeter from 0.7 to 90 GeV/c, both for the bare (5 cm) iron calorimeter and also when combined with the finely segmented lead scintillator calorimeter. In both cases there is a minimum response around 2 GeV/c. The cause of this is not completely understood but most probably stems from an energy dependence in the fraction of incident energy "lost" in nuclear excitation. Clearly it will be very instructive to see if a uranium calorimeter exhibits the same behaviour. It is possible to derive a calibration constant, which within the resolution of the device, can provide a good energy scale in the trigger, but fine tuning will demand a knowledge of whether or not one is dealing with a single high energy particle.

3.3. *Problems associated with 4π coverage*

In UA1 extensitve use will be made of the calorimeter information in order to apply a selective trigger determined from patterns of energy flow-total and transverse. At luminosities of $\sim 10^{30}\,\mathrm{cm^{-2}\,s^{-1}}$ the interaction rate will be $5 \times 10^4\,\mathrm{s^{-1}}$ which has to be matched selectively to a data acquisition speed of $10\,\mathrm{s^{-1}}$. If the energy based trigger is to make sense then the response and resolution of the calorimeters should not vary too strongly as a function of angle and point of incidence of the particles. Figure 25 shows the test data from prototypes taken with 60 GeV pions. The uninstrumented iron, and air gaps of the full UA1 calorimeter were simulated in the tests. The results from the trigger standpoint look very promising. At large angles one expects a worsening of the resolution because of the larger effective sampling steps, however this may be counterbalanced by improved containment. In terms of response, fewer plates in the detector are hit, but each receives a larger signal. These results indicate that with relatively simple geometries one can

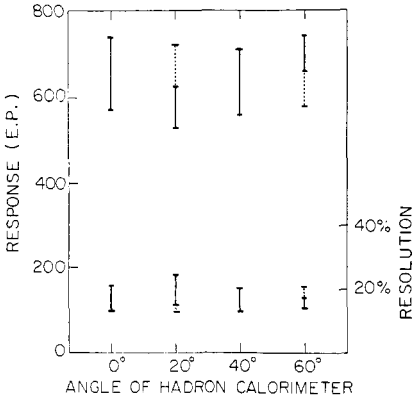

Fig. 25. Hybrid calorimeter response and resolution for incident pi minus of 60 GeV/c, as a function of angle of incidence to the hadron calorimeter.

probably meet the uniformity requirements, at least at the trigger level [± 15%]. The error bars in Fig. 25 represent the range in measured values and not the precision of a given measurement.

4. LEP physics and calorimetry

This is not a review of LEP physics potential – see for example J. Ellis at this meeting – nor is it an extensive statement of possible LEP experiments [12]. It is intended as an indication of the gain derived from good solid angle coverage ($\sim 4\pi$) with calorimetry on LEP experiments. By calorimetry one means both hadron and electromagnetic detectors. The hadron calorimeter not only serves to collect energy from neutral hadrons, e.g., K°, n, $\bar{n}$, etc., but when combined with a magnetic field and a good coordinate measurement outside, yields a muon spectrometer. A well segmented electromagnetic calorimeter provides an excellent discrimination between e/γ and pions. Another interesting feature of the full calorimetry is the detection of neutrinos by their lack of interaction and consequent energy imbalance, e.g., $W^+ \to e^+\nu$. Also the ability to collect the energy of jets could prove a very useful means of reconstructing the mass of W's via their copious two quark jet decays (80%). This facility is not so obviously attainable on hadron colliders, where high P_T background will probably swamp any signal.

4.1. *At the Z° pole*

Clearly if the Z° exists within the energy range of LEP a considerable amount of data will be collected at the pole, and attempts made to study decay modes with fully reconstructed events. Good calorimetry will be essential especially with its possible lepton identification (μ, e, ν), particularly if one is looking for new heavy leptons. The total visible energy will be a strong handle on each event.

4.2. *New flavours, onia*

The changes in event topology from jets produced from pairs of light quarks, to more isotropic events arising from the fragmentation of pairs of heavy quarks produced at thresholds, have been used extensively in searches at PETRA. The ability to add in neutral energy will sharpen these searches.

4.3. *W production*

The cross-section for single W production at LEP is extremely small $\sim 10^{-37}$ cm^2, and the experiment can only be considered, if the copious diquark decays of W's can be reconstructed from JET detection.

4.4. *W pairs*

At higher LEP energies this is a crucial reaction whose cross-section depends on the gauge group structure of the electro weak interaction. The signature may be very characteristic with four hadron jets from the decay of the W pair. The ability to "detect" the missing neutrino is vital in the recognition of W's via leptonic decays if one wishes to use all decay modes.

4.5. *Higgs particle*

The Higgs particle is intimately connected with the mass spectrum of elementary particles; its coupling strength to any object X is proportional to the mass of X, hence the Higgs may be produced in conjunction with heavy particles. It may show up in many ways at LEP, but possibly not with a clear characteristic decay; some possibilities for detection are:

(a) Heavy vector meson decay to a Higgs $V \to H\gamma$ – the emphasis will be on good high energy photon detection.

(b) $Z^\circ \to He^+e^-$, or $Z^\circ \to H\mu^+\mu^-$ – calorimetry can provide the lepton identification, and in the case of e^+e^-, the mass measurement.

(c) $e^+e^- \to ZH$ – here the Z must be reconstructed, possibly from pairs of jets, and the H inferred from missing mass.

None of these experiments is easy but without good 4π calorimetry some of them will be impossible. In addition, of course, one has a very useful indication on the possible contamination of events by two photon backgrounds.

5. Summary and conclusions

The performance of the major calorimetric components in the facilities are collected in Table I. The performance of some of the new facilities MAC, AFS, UA2, UA1 will give a good indication of what might be achieved at LEP with total calorimetry, where more and more one is dealing with the physics of quarks, through their fragmentation into collimated jets of comparatively low energy particles.

The possible particle identification and detection which comes with calorimetry has already been pointed out, in addition the ability to trigger on a particular amount of visible energy may prove very powerful in rejecting beam gas events – one watches UA1 with particular interest where the envisaged trigger depends on 4π calorimetry.

The problems which will have to be faced are numerous, 4π coverage with uniform response and resolution, calibration including a good knowledge of low energy response, and pattern recognition in calorimeters are a few obvious ones. In addition one feels that a LEP detector, which must run for a number of years, should be capable of some flexibility in its calorimetry as the physics emphasis may change, e.g., number of depth samples, change in size of readout channels, etc. It will remain a

Table I

Facility	Resolution
MARK J	Hadronic events r.m.s. ~ 20%, $\sqrt{s}$ = 30 GeV Large angle Bhabha σ ~ 10%, $\sqrt{s}$ = 30 GeV
JADE lead glass	± 6%/$\sqrt{E}$ for E < 6 GeV ± 3.8% at E = 15 GeV
TASSO liquid argon 2 mm Pb	± 5%, E > 4 GeV ± 10%/$\sqrt{E}$, 1 GeV < E < 4 GeV ± 15%/$\sqrt{E}$, $E \approx$ 0.3 GeV all with 1.3 rad lengths before detector
MAC Proportional tubes	
2.8 mm Pb	± 17%/$\sqrt{E}$, 0.5–15 GeV e's
2.7 cm Fe	± 75%/$\sqrt{E}$, 1–15 GeV π's
UA2 BBQ	
3.5 mm Pb	± 14%/$\sqrt{E}$
1.5 cm Fe	± 60%/$\sqrt{E}$ both measured with 1.5 radiation lengths of tungsten before the detector
UA1 BBQ	
1.2 mm Pb	± 13%/$\sqrt{E}$
4 mm Pb	± 10%/$\sqrt{E_T}$ (transverse energy)
5 cm Fe	± 80%/$\sqrt{E}$

challenge to the ingenuity of the physicists to retain this flexibility and yet remain within some reasonable financial constraints on the cost of the detector.

Acknowledgements

I should like to thank the following people for information concerning the performance of the facilities which they know and love F. Vannucci, R. Marshall, S. Orito, D. Saxon, P. Söding, J. M. Dorfan, R. Prepost, C. W. Fabjan and A. Clark. I am indebted to the organisers of this meeting for the opportunity to learn more about calorimetry performance.

References

1. M.I.T. Laboratory of Nuclear Science Report No. 107, April 1980.
2. JADE Collaboration, Bartel, W. et al., Phys. Lett. **88B**, 171 (1979).
3. PETRA Bulletin No. 14, April 1979.
4. Willis, W. J. and Radeka, V., NIM **120**, 221 (1974).
5. Anderson, R. L. et al., SLAC-PUB-2039 and IEEE 1977 Nuclear Science Symposium, San Francisco, October 19-21, IEEE **NS-25**, 340 1978.
6. A Proposal for a Lepton Total Energy Detector at PEP, (PEP-6), Anderson, R. L. et al.
7. Attwood, W. B. et al., SLAC Techm. Note SLAC-TN-76-7.
8. Fabjan, C. W. et al., NIM **141**, 61 (1977).
9. Darriulat, P. (spokesman) et al., CERN Proposal SPSC/78-8/P93.
10. Rubbia, C. (spokesman) et al., CERN Proposal SPSC/78-6/P92.
11. Corden, M. J. et al., Some Hadron Calorimeter Properties Relevant to Storage Rings, and Performance of UA1 Hadron Calorimeter Prototype, LEP Experimentation Meeting Uppsala, June 1980.
12. Proceedings of the LEP Summer Study, CERN 79.01.